HAL
open science

Atomic Structure of Epitaxial Graphene Sidewall Nanoribbons: Flat Graphene, Miniribbons, and the Confinement Gap

Irene Palacio, Arlensiú Celis, Maya N. Nair, Alexandre Gloter, Alberto Zobelli, Muriel Sicot, Daniel Malterre, Meredith S. Nevius, Walt A. de Heer, Claire Berger, et al.

To cite this version:

Irene Palacio, Arlensiú Celis, Maya N. Nair, Alexandre Gloter, Alberto Zobelli, et al.. Atomic Structure of Epitaxial Graphene Sidewall Nanoribbons: Flat Graphene, Miniribbons, and the Confinement Gap. Nano Letters, 2015, 15 (1), pp.182-189. 10.1021/nl503352v . hal-01271638

HAL Id: hal-01271638

https://hal.science/hal-01271638v1

Submitted on 24 Mar 2024

HAL is a multi-disciplinary open access archive for the deposit and dissemination of scientific research documents, whether they are published or not. The documents may come from teaching and research institutions in France or abroad, or from public or private research centers.

L'archive ouverte pluridisciplinaire **HAL**, est destinée au dépôt et à la diffusion de documents scientifiques de niveau recherche, publiés ou non, émanant des établissements d'enseignement et de recherche français ou étrangers, des laboratoires publics ou privés.

This is an open access article published under an ACS AuthorChoice License, which permits copying and redistribution of the article or any adaptations for non-commercial purposes.

NANO LETTERS

Letter

pubs.acs.org/NanoLett

Atomic Structure of Epitaxial Graphene Sidewall Nanoribbons: Flat Graphene, Miniribbons, and the Confinement Gap

Irene Palacio,[†] Arlensiú Celis,[‡,§] Maya N. Nair,[†] Alexandre Gloter,*[,‡] Alberto Zobelli,[‡] Muriel Sicot,[∥] Daniel Malterre,[∥] Meredith S. Nevius,[⊥] Walt A. de Heer,[⊥] Claire Berger,[⊥,#] Edward H. Conrad,[⊥] Amina Taleb-Ibrahimi,[†] and Antonio Tejeda*[,‡,§]

[†]UR1 CNRS/Synchrotron SOLEIL, Saint-Aubin, 91192 Gif sur Yvette, France

[‡]Laboratoire de Physique des Solides, Université Paris-Sud, CNRS, UMR 8502, F-91405 Orsay Cedex, France

[§]Synchrotron SOLEIL, L'Orme des Merisiers, Saint-Aubin, 91192 Gif sur Yvette, France

[∥]Université de Lorraine, UMR CNRS 7198, Institut Jean Lamour, BP 70239, F-54506 Vandoeuvre-lès-Nancy, France

[⊥]School of Physics, The Georgia Institute of Technology, Atlanta, Georgia 30332-0430, United States

[#]CNRS/Institut Néel, BP166, 38042 Grenoble, France

Supporting Information

ABSTRACT: Graphene nanoribbons grown on sidewall facets of SiC have demonstrated exceptional quantized ballistic transport up to 15 μm at room temperature. Angular-resolved photoemission spectroscopy (ARPES) has shown that the ribbons have the band structure of charge neutral graphene, while bent regions of the ribbon develop a bandgap. We present scanning tunneling microscopy and transmission electron microscopy of armchair nanoribbons grown on recrystallized sidewall trenches etched in SiC. We show that the nanoribbons consist of a single graphene layer essentially decoupled from the facet surface. The nanoribbons are bordered by 1−2 nm wide bent miniribbons at both the top and bottom edges of the nanoribbons. We establish that nanoscale confinement in the graphene miniribbons is the origin of the local large band gap observed in ARPES. The structural results presented here show how this gap is formed and provide a framework to help understand ballistic transport in sidewall graphene.

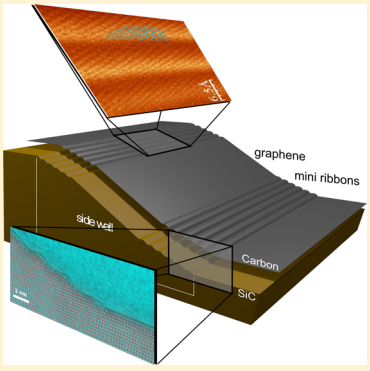

KEYWORDS: *Graphene, ribbon, atomic structure, band gap, HR-XTEM, STM*

High expectations are set for graphene electronics,[1] where the challenges are both transmitting the information with minimum losses (ballistic transport) and building conventional graphene FET digital devices by opening a band gap in graphene's π-bands. Tailoring graphene's shape was proposed to open a band gap in graphene by quantum confinement that led to a large effort to produce narrow graphene nanoribbons.[2−6] However, graphene-etched nanostructures are plagued by low mobility due to rough and disordered edges,[7−11] and the incompatibility of exfoliated ribbons with device production on an industrial scale. In fact, the problem of opening a band gap in graphene and the low electronic mobility of etched nanoribbons coupled with the manufacturability problem has resulted in a push to develop other 2D materials besides graphene for low dimensional electronics. We have previously shown that graphene nanoribbons grown on predetermined SiC steps[12] can be room-temperature ballistic conductors[13] and present a large local bandgap.[14] These edge-ordered graphene ribbons can be reproducibly patterned on a commercially viable insulating substrate and manufactured on scales compatible with industrial production,[12] opening up exciting real applications potential for graphene electronics. In this work, we determine the atomic structure of these sidewall ribbons, an important step toward the understanding of the mechanism of ballistic transport and why a band gap develops in these ribbons.

Epitaxial graphene on SiC is an industrially scalable platform on commercially available single-crystal wafers. It thus allows atomic control of both the graphene quality and its interface with the substrate. Lithography is used to produce very shallow steps on the SiC(0001) Si-face that define the graphene ribbon's boundaries and, combined with a thermal treatment to grow bottom-up graphene, results in well-defined smooth edges. Recently, 40 nm wide nanoribbons grown in this way on 4H-SiC facets[12] have demonstrated exceptional electronic properties with quantized ballistic transport up to 15 μm at room temperature[13] and evidence for an all graphene wide-bandgap semiconductor.[14] The ballistic channel propagates along the ribbon and the band gap is observed by ARPES at an angle consistent with the graphene bend at the top edge of the sidewall ribbon. Ballistic transport and a band gap are the most

Received: September 1, 2014
Revised: November 25, 2014
Published: December 2, 2014

Downloaded via 37.67.92.150 on March 24, 2024 at 17:02:04 (UTC).
See https://pubs.acs.org/sharingguidelines for options on how to legitimately share published articles.

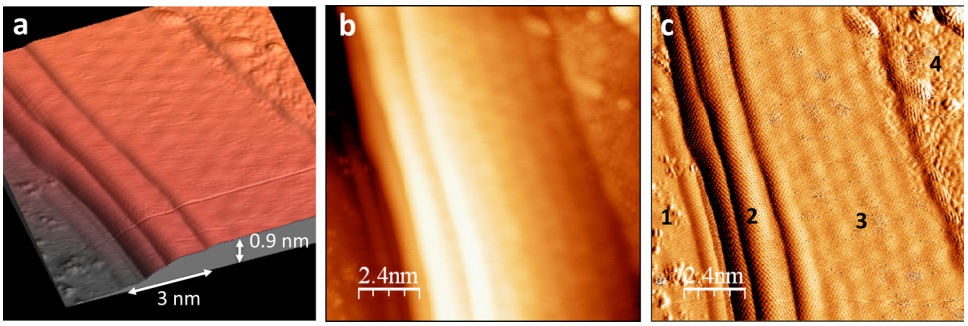

Figure 1. STM from a graphene nanoribbon on a natural SiC(0001) step. (a) Topographic three-dimensional STM image of a ribbon and its surroundings (V = 1.1 V, I = 0.7 nA). (b) Two-dimensional topographic image of (a). (c) Constant current image of (b). Region 1 is a precursor surface to graphene growth, region 2 is curved graphene on a natural step, region 3 is graphene overgrown on the plateau after the step, and region 4 is a region with another precursor state of graphene.

sought after ingredients for 2D electronics, making these discoveries a game-changing scenario for carbon electronics. However, no satisfactory explanation has been proposed so far to explain the observed properties. Local curvature effects, pn junctions, and strain have been suggested as the origin of the band gap. The main body of the ribbons, as measured by ARPES and STS, show that the electronic structure is that of charge neutral graphene,[13,15,16] different from the electronic structure in graphene grown on the flat Si-face of SiC (0001) plane.[17,18] In order to understand the single channel ballistic transport,[13] and why a large band gap appears in the sidewall ribbons, we need a detailed understanding of the nature of the edges, their orientation, and their termination into the buffer layer (the graphene layer at the SiC interface that is partially bonded to the SiC substrate) or into the SiC substrate. In this article, we examine the atomic and electronic structure of armchair epitaxial graphene sidewall ribbons. We show that ribbons on the $(1\bar{1}0n)$ and $(110n)$ facets are essentially flat and decoupled from the facet. More importantly, we show that facet graphene is unexpectedly bordered by miniribbons on both edges. Quantum confinement in the 1−2 nm wide miniribbons explains the observed bandgap. This work explains the origin of the band gap observed in ARPES and gives insight into the ballistic transport measurements.

As a reference, we first study graphene grown on a natural step (not on an artificial trench). Figure 1a shows a three-dimensional representation of a scanning tunneling microscopy (STM) image of graphene grown over a small $(1\bar{1}0n)$ natural step on the Si-face. The atomic topographic variations of the graphene honeycomb lattice of ∼6 pm are difficult to observe in standard two-dimensional images (Figure 1b) due to the 800 pm corrugation of the step. In order to observe simultaneously the honeycomb corrugation and the strong topographic variations, we use constant current imaging (Figure 1c). We can delineate four regions in the image. The first region (1) corresponds to the trench bottom where the graphene honeycomb is not well resolved (precursor region of the graphene growth). The second region (2) is graphene growing along the step edge up to the plateau and consists of multiple curves parallel to the step edge. In the third region (3), graphene overgrows the edge on the (0001) plateau. The overgrown graphene extends to a boundary with the fourth region, where another precursor state of graphene is observed (4).

STM images raise a number of important questions: What are the multiple curved graphene regions on the facets? What is their electronic structure? How are they different from the graphene on the flat (0001) plateaus? How are the structural elements related to the observed opening of a band gap in armchair (AC) ribbons?[14] What is the role of these different regions on transport along or perpendicular to the step direction? In this study, we begin to address these questions by making detailed structural measurements of graphene grown on reproducibly fabricated steps rather than random intrinsic steps in order to understand technologically relevant graphene nanoribbons. Here, we combine STM with high-resolution scanning transmission electron microscopy (STEM) in bright-field (BF), low- and high-angle annular dark-field (LAADF, HAADF) imaging modes. We thus access simultaneously the topography of the last atomic layer as well as the structure of any subsurface graphene and the graphene/SiC interface.

The studied arrays consist of 30−35 nm deep trenches etched in 4H-SiC (0001). The patterned substrate is annealed at 1100 °C for 30 min, followed by 1525 °C for a few minutes in a confinement controlled sublimation furnace.[12,14,19] The final result is a sample with an array of faceted mesa shapes shown in Figure 2. The first annealing step recrystallizes the vertical $(1\bar{1}00)$ or $(\bar{1}100)$ walls (depending on the original trench orientation) into the stable $(1\bar{1}0n)$ and $(\bar{1}10n)$ facets, respectively (Figure 2d). The final high-temperature growth step produces graphene. Both the (0001) plateaus and trench bottoms widths can be varied independently (Figure 2a,b) and the height difference between plateaus and trenches can also be tailored at will (Figure 2d). The height difference depends on the initial lithographic process and controls the width of the sidewall graphene nanoribbon that lies on the sidewall between the plateau and the trench. This ability to tailor the widths and edges opens up the possibility of tuning the electronic properties of the ribbons in a way that is compatible with mass production. Because of the orientational epitaxy of graphene grown on SiC(0001), the edge of the ribbons can be tuned. The AC edge of graphene will be oriented along the step edge of trench walls with $(1\bar{1}00)$ orientation. Conversely, trenches etched to give $(11\bar{2}0)$ walls will grow graphene with its zigzag (ZZ) edge parallel to the step edge of the trench wall. In this study, we focus on graphene nanoribbons with trench walls with $(1\bar{1}00)$ orientation, that is, AC edge graphene ribbons. Atomic resolution STM images confirm unambiguously that the trench orientation determines the armchair ribbon edge. Figure 3a−c shows the details of the graphene ribbon structure in the transition region between the sidewall and the plateau (zoom of the blue dashed rectangle in Figure 3b). In this

dx.doi.org/10.1021/nl503352v | Nano Lett. 2015, 15, 182−189

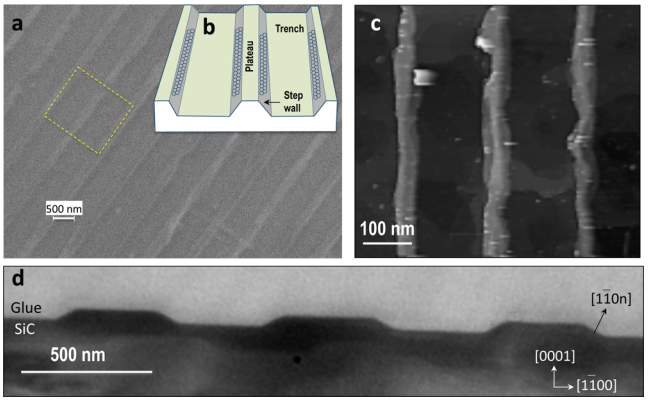

Figure 2. General overview of graphene nanoribbons grown on SiC (1$\bar{1}$0n) and SiC (1$\bar{1}$0n) facets (sidewall ribbons). (a) Scanning electron microscopy image showing the general topography of the artificial graphene ribbon array. The brightest and darkest parts correspond to plateaus and trenches, respectively. Sidewall graphene ribbons are on the sidewall, as sketched in (b) corresponding to the dashed yellow rectangle in the SEM image. Plateau's width is 250 nm. (c) STM image (4 V, 0.1 nA) showing the regions with [0001] normal, that is, the trenches and plateaus. Plateau's width is 30 nm. (d) Cross-sectional TEM image of the array of ribbons in another sample. Plateaus width of 300 nm.

transition region, the surface normal changes from (1$\bar{1}$07) to the (0001) flat surface. The graphene honeycomb structure is seen both along the oscillations and on a strip partially extending onto the (0001) surface. As shown below using cross-sectional STEM, the oscillations correspond to graphene draping over SiC minifaceting.

Figure 3d–g shows STEM-HAADF and STEM-LAADF views of a faceted step patterned on SiC. The STEM-HAADF imaging mode clearly displays the atomic structure of the SiC substrate, while the STEM-LAADF is more sensitive to carbon-based material, thus enhancing the contrast of the graphene ribbons and showing the presence of a single graphene layer (Figure 3e). Figure 3d,e shows atomically resolved STEM images with a large field of view of the sidewall; two main families of facets are observed. First, the central part of the sidewall (tens of nanometers wide) has a normal rotated ca. 30° with respect to the SiC (0001) plane (corresponding to a [1$\bar{1}$07] surface). Second, the top and bottom part of the sidewall are composed of facets tilted ∼20° from the (0001) plane corresponding to $[1\bar{1}0n]_{n=9,10}$ planes (Figure 3d). An expanded view of the upper region of the sidewall in Figure 3d,e shows more details (Figure 3f-g). The upper part of the sidewall is composed of a series of several small (0001) miniterraces and minifacets due to the fracturing of the initial facet during graphene growth.[20] The minifacets typically have a [1$\bar{1}$05] orientation extending over 4 SiC bilayers along the [0001] orientation, that is, the unit cell of 4H-SiC. Graphene grows continuously over all the minifacets as well as along the central extended (flat) facet, while bonding from time to time

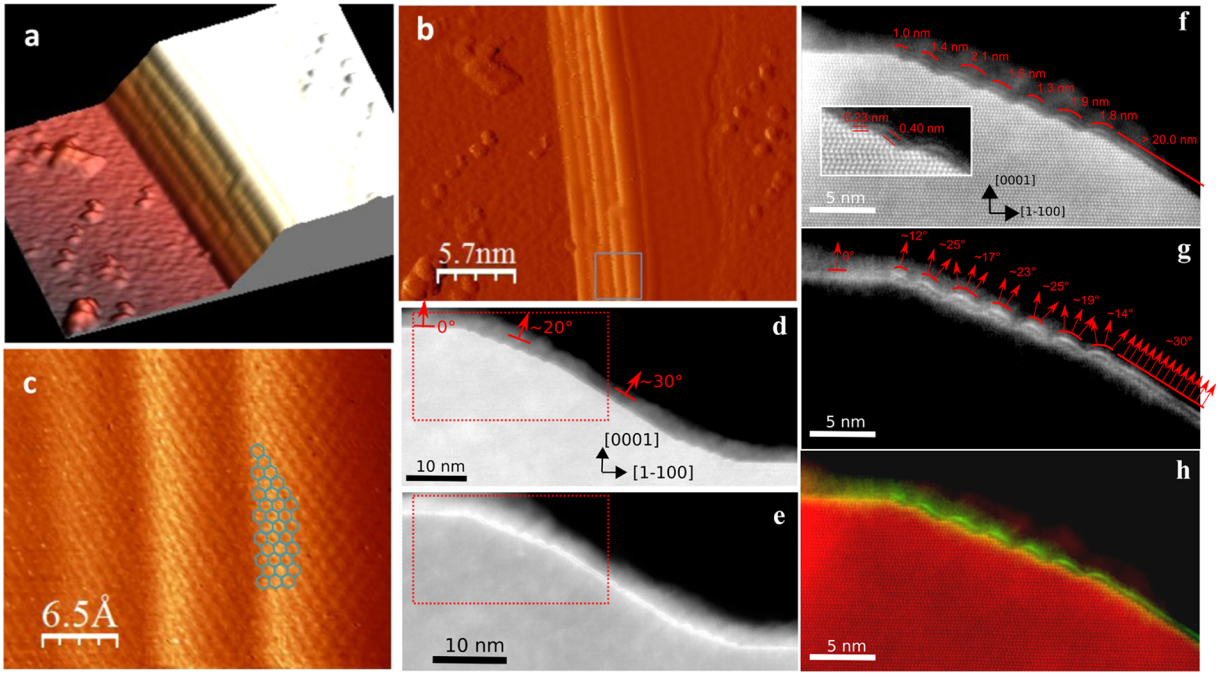

Figure 3. Top and cross section views of a graphene sidewall ribbon. (a) Three-dimensional STM image of a 3.3 nm height sidewall showing undulations on the sidewall. (b) STM constant current image of (a). (c) Detail of the connection between sidewall and plateau regions, showing the continuity of graphene all across the boundaries despite the oscillations at the minifacets. The armchair edge of the ribbon runs parallel to the sidewall edge (see the Supporting Information for another image with better resolution). (d) STEM-HAADF image of the sidewall. The lower and the upper parts of the sidewall have an average normal of around 20° from the [0001] direction. In between, there is a region with a normal 30° off the [0001] direction. (e) STEM-LAADF image of the same sidewall as in (d). Carbon layers and defective or strained area at the SiC give larger contrast in LAADF mode and thus can be identified on the facet wall. (f) Zoom of (d) in the region indicated by the red rectangle. The region with 20° average normal is constituted by minifacets where graphene floats in a 1.5–2 nm region. The inset shows a detail of a miniribbon. A floating graphene region is pinned between two miniterraces where graphene is bonded to the substrate. (g) The parts where graphene is floating are curved regions with normals ranging between 15° and 25° off the [0001] direction. (h) False-color image of a minifacet region where red enhances the SiC visible by HAADF and green highlights the graphene as imaged by LAADF.

dx.doi.org/10.1021/nl503352v | Nano Lett. 2015, 15, 182–189

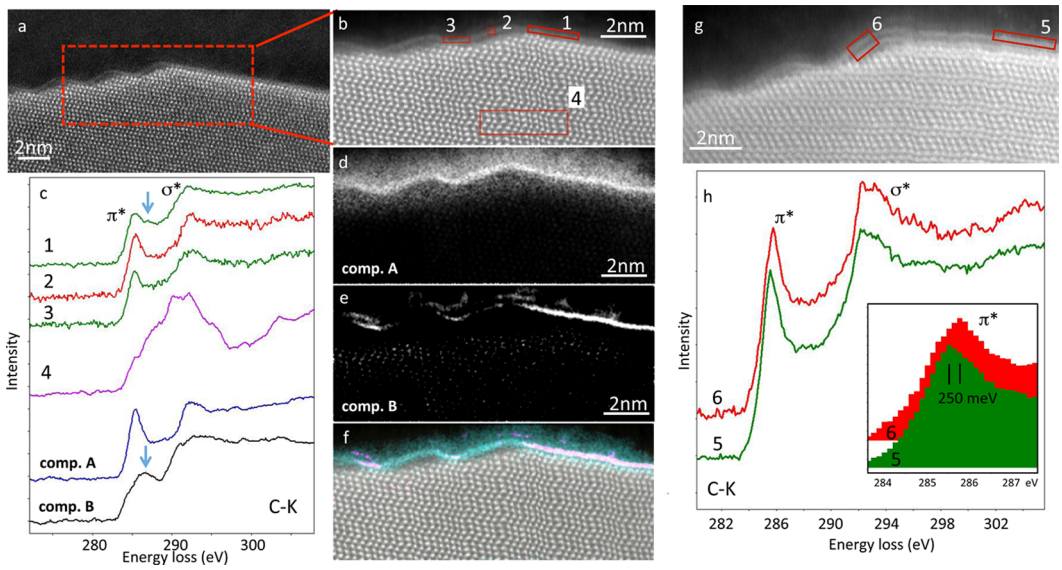

Figure 4. STEM-EELS analysis at the carbon K-edge for a monolayer (a–f) and bilayer (g–h) ribbons. (a) STEM-HAADF image of the boundary between miniribbons and plateau in a single layer ribbon. The rectangle indicates the chosen area for STEM-EELS spectromicroscopy measurement. (b) STEM-HAADF image obtained during the spectromicroscopy measurement. The boxes 1–4 show the regions corresponding to spectra in (c). (c) Raw spectra extracted from the buffer layer (spectrum 1), the first miniribbon (spectrum 2), the miniterrace (spectrum 3) and the SiC bulk (spectrum 4). Component A and B spectra represent the main spectral components related to the carbon layer at the surface of the SiC. (d) Spatial location of the component A, typical of graphene. (e) Spatial location of the component B, compatible with a band gap opening. (f) Pseudocolor image where gray enhances the SiC and cyan highlights the graphene and the perturbated SiC. (g) STEM-HAADF image obtained during STEM-EELS measurement showing the boundary between miniribbons and plateau in the case of bilayer ribbon. The boxes 5–6 indicate the regions where spectra have been extracted. A STEM-HAADF image of the whole sidewall can be seen in Supporting Information Figure S4. (h) EELS spectra for graphene (spectrum 5) and miniribbon (spectrum 6). The inset shows an energy shift to the higher energy of ca. 250 meV of the π^* excitation for a miniribbon with respect to the graphene.

to the substrate. In particular, graphene draping over the minifacets is pinned to the substrate at both edges (in the upper and at the bottom parts, see inset in Figure 3f) while leaving a curved floating graphene layer of a typical width between 1.5 to 2 nm (Figure 3f). The distance of the graphene layer to the substrate in the pinned miniterraces is 2.3 Å, a distance characteristic of the tightly bound buffer layer on the Si (0001) face. In between the pinned regions, the graphene is curved and seems to be "floating", as its distance to the substrate is extremely high (4.0 Å). This causes the graphene in the bend to electronically decouple from the SiC (see below) and thus forms a narrow AC-edge graphene ribbon running parallel to the SiC step edge. The distribution of the local normal orientation in the curved region ranges from ca. 15° to 25° depending on the different minifacet height (Figure 3g). In the flat extended facet, graphene spreads over a width of 20 nm in a more regular 30° normal orientation (Figure 3d). The facet is flat and the graphene layer is at an average distance of ca. 3.5 Å from the substrate, which is much larger than the 2.3 Å distance for the tightly bonded buffer layer. This clearly indicates that the nanoribbon is essentially decoupled from the substrate (or delaminated[21]), apart from sparse more or less regularly spaced anchored points. The quality of graphene on this facet is indicated by the STEM-LAADF contrast. Note that the $(1\bar{1}0n)$ and $(\bar{1}10n)$ are nonpolar, which may explain[22] why the nanoribbons are charge neutral.[13,14]

Figure 3h superimposes colorized STEM-LAADF and STEM-HAADF images to clarify the position of the graphene ribbons with respect to the SiC substrate. The image shows that the (0001) SiC planes located at the bottom trench and at the top plateau are covered by a carbon layer located at a distance of ~2.3–2.8 Å from the SiC, typical for the buffer graphene layer.[23–25] Similar tightly bonded layers can also be seen in the mini (0001) terraces.

Other STEM (BF, HAADF, LAADF) and TEM-BF images from similar monolayer ribbons in the Supporting Information (Figure S2) confirm the reproducibility of these results, as already inferred from the ARPES measurements performed on several hundreds of sidewall.[14] Previous results were obtained on monolayer ribbons. Bilayer ribbons are less likely but have also been observed (see Supporting Information Figure S3). In this case, the structure of the sidewall remains essentially unchanged from the one-layer films discussed above. There are still minifacets at the top and bottom separated by a large extended flat facet in between and a second continuous graphene layer drapes from the top to the bottom of the sidewall as shown in the Supporting Information. The spacing between the two graphene layers is ca. 3.5 Å, which is slightly larger than in normal graphite as was observed in previous TEM experiments.[23] This can be qualitatively understood if the two layers are Bernal stacked on the (0001) plateau, as is the case for Si-face bilayers, as there may no longer be registry along the facet due to the top sidewall curvature. A larger graphene layer separation is commonly observed for non-Bernal stacked graphene layers, such as the epitaxial graphene on the carbon $(000\bar{1})$ face.[26]

These structural studies confirm the orientation of the facets that was determined by angle-resolved photoemission, as well as the presence of a curved region. Angle-resolved photoemission has observed a linear dispersion at the $(1\bar{1}07)$ extended facet. No band gap was observed within the 50 meV resolution[14] (the uncertainty in the Fermi level position). This band structure is consistent with the STEM observation for the large central ribbon (electronically decoupled from the regions

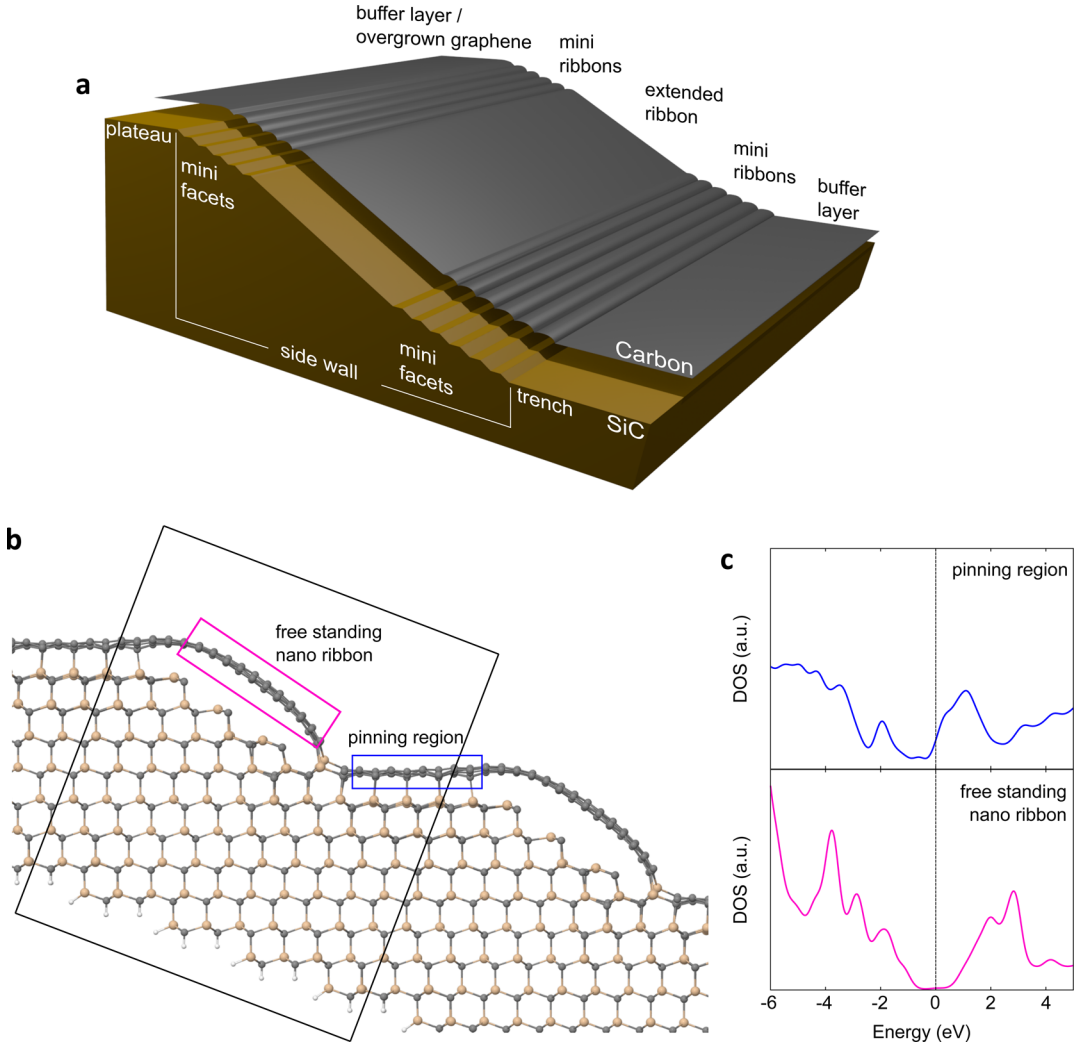

Figure 5. Modelization of the atomic structure and density of states. (a) Schematics of the model proposed for the general structure of armchair graphene ribbons grown on SiC, Si-face. The sidewall is composed of an extended facet in between a bottom and a top series of minifacets. On top of the sidewall a continuous graphene sheet grows and exhibits different normals depending on the region. The extended facet corresponds to a 30° off normal with respect to the SiC (0001) plane (corresponding to $[1\bar{1}07]$ surface), the minifacets have a normal tilted ∼20° from the (0001) plane, corresponding to $[1\bar{1}0n]_{n=9,10}$ planes. In the (0001) miniterraces of the minifacets, graphene is bonded to the substrate. In between these pinning areas, graphene is floating without any strain and exhibits a band gap. The band gap is due to the quantum confinement in the miniribbon. (b) Relaxed atomic positions of single-layer graphene miniribbons at SiC facet with [0001] and $[1\bar{1}05]$ orientations. (c) Density of states at the positions indicated in (b). Top panel: floating graphene in the electronically decoupled miniribbon. Bottom panel: gapped and doped buffer layer with some interface states in the gap.

with the minifacets) because its width will not produce an observable gap. Interestingly, ARPES measurements[14] have determined that some regions with normal intermediate between [0001] and $[1\bar{1}07]$ have a band gap of at least 500 meV. There are several possibilities why a band gap would open in these graphene ribbons. Uniaxial strain can open a gap in armchair ribbons when the strain is perpendicular to the edge[27,28] but in order to explain the experimental gap bonds should be strained by an unphysical, large value of more than 20%. Nevertheless, STEM images show that graphene in the miniribbons "floats" between the pinning miniterraces, that is, the graphene layer is able to relax any residual strain, which rules out a strain-induced gap. A more realistic possibility is quantum confinement in the narrow miniribbons that border the main facet. With a 1−2 nm width, band gaps of 0.5−1 eV can be expected.[29] In order to confirm that the ARPES observed band gap is effectively spatially located in the curved graphene miniribbons, we performed STEM-EELS measurement. We focus on the carbon K-edges corresponding to transitions between the C 1s core electron to the unoccupied density of states just above the Fermi level (Figure 4).

The boundary between the plateau and the miniterraces covered with a graphene monolayer is shown in Figure 4a. The buffer layer at the SiC top surface and two miniribbons separated by miniterraces can be observed. Figure 4b is a zoomed in image of the area boxed in Figure 4a where a spectromicroscopy measurement was performed. EELS spectra were collected with a spatial step of 0.04 nm and an acquisition time of several milliseconds. Spectra integrated in the boxes of Figure 4b are characteristic of different regions (Figure 4c): the buffer layer (position 1), the miniribbon (position 2), and the miniterrace (position 3). The spectrum from the miniribbon shows the π^* and σ^* peaks characteristic of graphene or graphite-like materials.[21] The spectra from the buffer layer and

dx.doi.org/10.1021/nl503352v | Nano Lett. 2015, 15, 182−189

the miniterrace have noticeable additional spectral intensity in between the π^* and σ^* peaks (located ca. 1.3 eV higher in energy than the π^*, as indicated by an arrow in the case of the buffer layer, spectrum 1 in Figure 4c). To isolate the additional features in the buffer and miniterrace, we have analyzed the main spectral components in the EELS spectra by using spectral unmixing based on a Vertex component analysis.[30] The two spectral components of the EELS spectra (A and B) are shown in Figure 4c. Figure 4d,e shows the spatial distribution of components A and B respectively. Component A is observed all along the carbon atomic layer, and it is thus associated with graphene/graphite. On the other hand, an additional component B, which exhibits a strong peak ca. 1.3 eV above the graphene π^* peak, is only present when the C-layer is strongly bounded to the SiC surface (i.e., at either the buffer layer or the miniterraces). STS measurements and ab initio calculations[31] have indicated that the buffer layer has a small band gap with the presence of additional spatially localized in-gap states associated with the complex hybridization between the buffer layer and the SiC surface. These peculiar electronic structures might be the origin of the additional spectral component B found in the buffer layer and also at the miniterraces. Whatever the exact origin of this EELS spectral component B, it confirms that the electronic structure at both sides of miniribbons is different from that of pure graphene/graphite.

In order to explore the differences in the electronic structures of the miniribbons and the more extended graphene ribbon, we have investigated EELS spectra at higher resolution. Figure 4g shows a region on the plateau where overgrown graphene can be distinguished above the buffer layer (see Supporting Information Figure S3 for the detailed structure of this step). This graphene layer above the buffer layer is known to be metallic.[24] The EELS spectrum of this layer (measured at position 5 in Figure 4g) compared with that of the miniribbons in the same image (position 6), shows a different shape of the π^* and an energy shift of around 0.25 eV. A similar difference in π^* excitations has been recently reported between semiconducting and metallic nanotubes by XAS and EELS spectroscopy.[32] The observed energy shift thus confirms that the electronically decoupled miniribbons exhibit a band gap. All these results demonstrate that the electronic properties of the sidewall graphene are significantly modified near the top and bottom edges of the facet. At these points on the sidewall, small minigraphene ribbons form. The center of the miniribbons is detached from the SiC while their edges are bonded to the substrate. The edges behave like a normal (0001) buffer graphene layer. These buffer layer strips isolate the graphene in between, creating electronic confinement that opens a significant bandgap in the miniribbons [see Figure 5a].

A quantum confinement induced band gap was predicted for certain width AC edge ribbons using a tight binding model.[33] Higher level calculations predict that both AC and ZZ edge graphene ribbons would be semiconductors.[29,34] As we will show using complementary numerical simulations conducted in the framework of density functional theory, the confined miniribbons observed in these studies also have a bandgap. The surface corresponding to $[1\bar{1}010]$ at the top and bottom region of the sidewall have been modeled by a 1.7 nm thick SiC slab where the lower surface has been saturated by hydrogen atoms. The supercell periodicity has been chosen along the $[\bar{1}\bar{1}010]$ step edge direction in order to minimize the strain on the graphene ribbons; three armchair graphene periods are accommodated over four SiC step periods leading to a graphene compression as low as 3.6%. This compression relaxes through a slight out-of-plane rippling of the miniribbons. A 2.9 nm wide graphene sheet is considered in each minifacet. A 1.1 nm portion of this sheet is located on top of the SiC miniterraces (buffer layer) and 1.8 nm are free-standing. The fully relaxed 806 atoms model is displayed in Figure 5b.

The projected density of states of the system is presented in Figure 5c. The buffer layer at the miniterraces has a projected density of states shifted with respect to the free-standing ribbons, which is in agreement with previous results on extended buffer layers.[31,35] The free-standing graphene region presents an LDA electronic gap of about 1 eV (Figure 5c). This energy gap is on the order of magnitude of the expected gap for free-standing armchair ribbons with similar widths. In the ideal case, the band gap decreases with increasing ribbon width. A $3N$ quasi-period oscillation superposes on this trend (N the number of carbon dimer lines across the ribbon width). Edge functionalization conserves the overall quasi-periodic width/band gap dependence while introducing a phase shift.[29] The electronic behavior of the complex SiC/graphene heterostructure can be linked to the simpler case of quantum confinement in free-standing ribbons with specific edge functionalizations. The 0.25 eV energy shift observed for the π^* carbon edge in the graphene miniribbon is almost certainly related to these quantum confinement effects. In fact, quantum confinement also induces strong width-dependent excitonic effects with respect to ground-state electronic structures, strongly decreasing the onset of optical measurements and EELS core edges.[36,37] This explains the observed energy shift in EELS spectra, which is much smaller than the band gap opening expected for few nanometer width ribbons.

In summary, we present STM and cross-sectional STEM studies of armchair edge nanoribbons grown on recrystallized sidewall trenches etched in SiC. The main result is that the unusual and reproducible facet geometry, coupled with how the graphene grows on the facet, explains that the band gap observed in ARPES is due to a finite size effect caused by 1−2 nm wide nanoribbons with ordered edges.

We show that after etching a step in a SiC (0001) surface, the trench walls facet into a central extended flat SiC $(1\bar{1}07)$ or SiC $(\bar{1}107)$ facet that is tens of nanometers wide. This facet is bordered on both sides by much smaller but regular minifacets. A honeycomb graphene layer drapes over the whole sidewall. The graphene that grows on the main facet is of high quality and is essentially decoupled from the substrate, which is consistent with the charge neutral graphene band structure observed in ARPES. In addition, the main facet graphene is the probable location for ballistic transport observed in sidewall graphene. On the bordering nanofacets, miniribbons 1−2 nm wide form. Miniribbons are defined by boundaries where they attach to graphene tightly bonded to the (0001) oriented nanoterraces. The tightly bonded graphene on the (0001) nanoterraces shows properties similar to that of the graphene buffer layer. In between these pinning terraces, graphene is curved and decoupled from the substrate.

The location of the miniribbons and EELS results are consistent with the band gap observed in ARPES. Ab initio calculations confirm that this band gap results from electronic confinement in these electronically decoupled miniribbons. This observation opens an interesting perspective in terms of tailoring the graphene band gap. Changing the SiC polytype

and therefore the *c*-axis periodicity could result in various crystallographic nanofaceting and in turn, different miniribbon widths that would determine the band gap.

Our structural determination of the sidewall ribbon geometry is particularly relevant when correlated to their electronic properties. Coupling structure to electronic properties is fundamental for a thorough understanding of the system giving new and real perspectives for their applications. The reproducible and scalable geometry on commercially available wafers allows for several interesting device fabrication possibilities. Taking advantage of the set of semiconducting ribbons, metal−semiconducting−metal junctions could be realized with source-drain contacts on the metallic graphene at the top (0001) surface and the metallic part of the facet, respectively. Other interesting possibilities include devices parallel to the step edges, along the ballistic transport direction for interconnects. In conclusion, the sidewall ribbon geometry offers many new architectures that are assured to stimulate new graphene device structures.

■ ASSOCIATED CONTENT

Supporting Information

Full experimental methods, statistical analysis of the structure of sidewall ribbons by STEM, and high-resolution STM image of ribbons edge. This material is available free of charge via the Internet at http://pubs.acs.org.

■ AUTHOR INFORMATION

Corresponding Authors

*E-mail: gloter@lps.u-psud.fr.

*E-mail: tejeda@lps.u-psud.fr.

Notes

The authors declare no competing financial interest.

■ ACKNOWLEDGMENTS

This work was supported by the French Agence Nationale de la Recherche (ANR), project CoRiGraph, ref ANR-12-BS04-0017 and by the French American Cultural Exchange council through a Partner University Fund project. E.H.C. acknowledges support from the National Science Foundation under Grant DMR-1005880. Support from the NSF No. DMR-0820382, AFSOR, and Keck foundation is also acknowledged. C.B. acknowledges partial funding from the European graphene flagship.

■ REFERENCES

(1) Berger, C.; Song, Z.; Li, T.; Li, X.; Ogbazghi, A. Y.; Feng, R.; Dai, Z.; Marchenkov, A. N.; Conrad, E. H.; First, P. N.; de Heer, W. A. Ultrathin Epitaxial Graphite: 2D Electron Gas Properties and a Route toward Graphene-based Nanoelectronics. *J. Phys. Chem. B* **2004**, *108*, 19912−19916.

(2) Tao, C.; Jiao, L.; Yazyev, O. V.; Chen, Y.-C.; Feng, J.; Zhang, X.; Capaz, R. B.; Tour, J. M.; Zettl, A.; Louie, S. G.; Dai, H.; Crommie, M. F. Spatially resolving edge states of chiral graphene nanoribbons. *Nat. Phys.* **2011**, *7*, 616−620.

(3) Chen, Z.; Lin, Y. M.; Rooks, M. J.; Avouris, P. Graphene nanoribbon electronics. *Physica E* **2007**, *40*, 228.

(4) Han, M. Y.; Özyilmaz, B.; Zhang, Y.; Kim, P. Energy band-gap engineering of graphene nanoribbons. *Phys. Rev. Lett.* **2007**, *98*, 206805.

(5) Cai, J.; Ruffieux, P.; Jaafar, R.; Bieri, M.; Braun, T.; Blankenburg, S.; Muoth, M.; Seitsonen, A. P.; Saleh, M.; Feng, X.; Müllen, K.; Fasel, R. Atomically precise bottom-up fabrication of graphene nanoribbons. *Nature* **2010**, *466*, 470−473.

(6) Li, Y. Y.; Chen, M. X.; Weinert, M.; Li, L. Direct experimental determination of onset of electron−electron interactions in gap opening of zigzag graphene nanoribbons. *Nat. Commun.* **2014**, *5*, 4311.

(7) Areshkin, D. A.; Gunlycke, D.; White, C. T. Ballistic Transport in Graphene Nanostrips in the Presence of Disorder: Importance of Edge Effects. *Nano Lett.* **2007**, *7*, 204−210.

(8) Querlioz, D.; Apertet, Y.; Valentin, A.; Huet, K.; Bournel, A.; Galdin-Retailleau, S.; Dollfus, P. Suppression of the orientation effects on bandgap in graphene nanoribbons in the presence of edge disorder. *Appl. Phys. Lett.* **2008**, *92*, 042108.

(9) Cresti, A.; Roche, S. Edge-disorder-dependent transport length scales in graphene nanoribbons: From Klein defects to the superlattice limit. *Phys. Rev. B* **2009**, *79*, 233404.

(10) Sols, F.; Guinea, F.; CastroNeto, A. H. Coulomb blockade in graphene nanoribbons. *Phys. Rev. Lett.* **2007**, *99*, 166803.

(11) Han, M. Y.; Brant, J. C.; Kim, P. Electron transport in disordered graphene nanoribbons. *Phys. Rev. Lett.* **2010**, *104*, 056801.

(12) Sprinkle, M.; Ruan, M.; Hu, Y.; Hankinson, J.; Rubio-Roy, M.; Zhang, B.; Wu, X.; Berger, C.; de Heer, W. A. Scalable templated growth of graphene nanoribbons on SiC. *Nat. Nanotechnol.* **2010**, *5*, 727−731.

(13) Baringhaus, J.; Ruan, M.; Edler, F.; Tejeda, A.; Sicot, M.; Taleb Ibrahimi, A.; Jiang, Z.; Conrad, E. H.; Berger, C.; Tegenkamp, C.; de Heer, W. A. Exceptional ballistic transport in epitaxial graphene nanoribbons. *Nature* **2014**, *506*, 349.

(14) Hicks, J.; Tejeda, A.; Taleb-Ibrahimi, A.; Nevius, M. S.; Wang, F.; Shepperd, K.; Palmer, J.; Bertran, F.; Le Fèvre, P.; Kunc, J.; de Heer, W. A.; Berger, C.; Conrad, E. H. A wide-bandgap metal−semiconductor−metal nanostructure made entirely from graphene. *Nat. Phys.* **2013**, *9*, 49−54.

(15) Sprinkle, M.; Siegel, D.; Hu, Y.; Hicks, J.; Tejeda, A.; Taleb-Ibrahimi, A.; Le Fèvre, P.; Bertran, F.; Vizzini, S.; Enriquez, H.; Chiang, S.; Soukiassian, P.; Berger, C.; de Heer, W. A.; Lanzara, A.; Conrad, E. H. First Direct Observation of a Nearly Ideal Graphene Band Structure. *Phys. Rev. Lett.* **2009**, *103*, 226803.

(16) Tejeda, A.; Taleb-Ibrahimi, A.; de Heer, W.; Berger, C.; Conrad, E. H. Electronic structure of epitaxial graphene grown on the C-face of SiC and its relation to the structure. *New J. Phys.* **2012**, *14*, 125007.

(17) Bostwick, A.; Ohta, T.; Seyller, T.; Horn, K.; Rotenberg, E. Quasiparticle dynamics in graphene. *Nat. Phys.* **2006**, *3*, 36.

(18) Zhou, S. Y.; Gweon, G. H.; Fedorov, A. V.; First, P. N.; de Heer, W. A.; Lee, D. H.; Guinea, F.; Castro Neto, A. H.; Lanzara, A. Substrate-induced bandgap opening in epitaxial graphene. *Nat. Mater.* **2007**, *6*, 770.

(19) de Heer, W. A.; Berger, C.; Ruan, M.; Sprinkle, M.; Li, X.; Hu, Y.; Zhang, B.; Hankinson, J.; Conrad, E. H. Large area and structured epitaxial graphene produced by confinement controlled sublimation of silicon carbide. *Proc. Natl. Acad. Sci. U.S.A.* **2011**, *108*, 16900−16905.

(20) Ming, M.; Zangwill, A. Model and simulations of the epitaxial growth of graphene on non-planar 6H−SiC surfaces. *J. Phys. D: Appl. Phys.* **2012**, *45*, 154007.

(21) Nicotra, G.; Ramasse, Q. M.; Deretzis, I.; La Magna, A.; Spinella, C.; Giannazzo, F. Delaminated Graphene at Silicon Carbide Facets: Atomic Scale Imaging and Spectroscopy. *ACS Nano* **2013**, *7*, 3045.

(22) Ostler, M.; Deretzis, I.; Mammadov, S.; Giannazzo, F.; Nicotra, G.; Spinella, C.; Seyller, T.; La Magna, A. Direct growth of quasi-free-standing epitaxial graphene on nonpolar SiC surfaces. *Phys. Rev. B* **2013**, *88*, 085408.

(23) Norimatsu, W.; Kusunoki, M. Transitional structures of the interface between graphene and 6H−SiC (0 0 0 1). *Chem. Phys. Lett.* **2009**, *468*, 52−56.

(24) Emtsev, K. V.; Speck, F.; Seyller, Th.; Ley, L.; Riley, J. D. Interaction, growth, and ordering of epitaxial graphene on SiC{0001} surfaces: A comparative photoelectron spectroscopy study. *Phys. Rev. B* **2008**, *77*, 155303.

(25) Riedl, C.; Starke, U.; Bernhardt, J.; Franke, M. Structural properties of the graphene-SiC(0001) interface as a key for the preparation of homogeneous large-terrace graphene surfaces. *Phys. Rev. B* **2007**, *76*, 245406.

(26) Sprinkle, M.; Hicks, J.; Tejeda, A.; Taleb-Ibrahimi, A.; Le Fèvre, P.; Bertran, F.; Tinkey, H.; Clark, M. C.; Soukiassian, P.; Martinotti, D.; Hass, J.; Conrad, E. H. Multilayer epitaxial graphene grown on the SiC (000−1) surface; structure and electronic properties. *J. Phys. D: Appl. Phys.* **2010**, *43*, 374006.
(27) Wong, J.-H.; Wu, B.-R.; Lin, M.-F. Strain Effect on the Electronic Properties of Single Layer and Bilayer Graphene. *J. Phys. Chem. C* **2012**, *116*, 8271−8277.
(28) Pereira, V.; Castro Neto, A.; Peres, N. A tight-binding approach to uniaxial strain in graphene. *Phys. Rev. B* **2009**, *80*, 045401.
(29) Wagner, P.; Ewels, C. P.; Adjizian, J. J.; Magaud, L.; Pochet, P.; Roche, S.; Lopez-Bezanilla, A.; Ivanovskaya, V. V.; Yaya, A.; Rayson, M.; Briddon, P.; Humbert, B. Band Gap Engineering via Edge-Functionalization of Graphene Nanoribbons. *J. Phys. Chem. C* **2013**, *117*, 26790.
(30) Dobigeon, N.; Brun, N. Spectral mixture analysis of EELS spectrum- images. *Ultramicroscopy.* **2012**, *120*, 25.
(31) Kim, S.; Ihm, J.; Choi, H. J.; Son, Y.-W. Origin of Anomalous Electronic Structures of Epitaxial Graphene on Silicon Carbide. *Phys. Rev. Lett.* **2008**, *100*, 176802.
(32) Rossouw, D.; Botton, G. A.; Najafi, E.; Lee, V.; Hitchcock, A. P. Metallic and Semiconducting Single-Walled Carbon Nanotubes: Differentiation individual SWCNT by their Carbon 1s Spectra. *ACS Nano* **2012**, *6*, 10965.
(33) Wakabayashi, K.; Fujita, M.; Ajiki, H.; Sigrist, M. Electronic and Magnetic Properties of Nanographite Ribbons. *Phys. Rev. B* **1999**, *59*, 8271−8282.
(34) Son, Y.-W.; Cohen, M. L.; Louie, S. G. Energy Gaps in Graphene Nanoribbons. *Phys. Rev. Lett.* **2006**, *97*, 216803−4.
(35) Varchon, F.; Feng, R.; Hass, J.; Li, X.; Ngoc Nguyen, B.; Naud, C.; Mallet, P.; Veuillen, J. Y.; Berger, C.; Conrad, E. H.; Magaud, L. Electronic Structure of Epitaxial Graphene Layers on SiC: Effect of the Substrate. *Phys. Rev. Lett.* **2007**, *99*, 126805.
(36) Prezzi, D.; Varsano, D.; Ruini, A.; Marini, A.; Molinari, E. Optical properties of graphene nanoribbons: The role of many-body effects. *Phys. Rev. B* **2009**, *77*, 041404.
(37) Prezzi, D.; Varsano, D.; Ruini, A.; Molinari, E. Quantum dot states and optical excitations of edge modulated graphene nanoribbons. *Phys. Rev. B* **2011**, *84*, 041401.